Froehlich, K.; Nasir, S.; Ali, M.; Ramirez Hoyos, P.; Cervera, J.; Mafe, S.; Ensinger, W. (2021). Fabrication of soft-etched nanoporous polyimide membranes for ionic conduction and discrimination. Journal of Membrane Science. 617:1-9. https://doi.org/10.1016/j.memsci.2020.118633

Fabrication of Soft-Etched Nanoporous Polyimide Membranes for Ionic Conduction and Discrimination

Kristina Froehlich[a,#], Saima Nasir[a,b,#], Mubarak Ali[a,b,*], Patricio Ramirez[c], Javier Cervera[d], Salvador Mafe[d], and Wolfgang Ensinger[a]

[a]*Dept. of Material- and Geo-Sciences, Materials Analysis, and Center of Synthetic Biology, Technische Universität Darmstadt, Alarich-Weiss-Str. 02, D-64287 Darmstadt, Germany*

[b]*Materials Research Department, GSI Helmholtzzentrum für Schwerionenforschung, Planckstrasse 1, D-64291, Darmstadt, Germany*

[c]*Dept. de Física Aplicada. Univ. Politècnica de València. E-46022 Valencia, Spain*

[d]*Dept. de Física de la Terra i Termodinàmica, Universitat de València, E-46100 Burjassot, Spain*

# Equal contributions

*Corresponding authors:

Email address: m.ali@gsi.de

ABSTRACT

Ionic selectivity in nanopores is usually based either on steric or charge exclusion mechanisms. By simultaneously incorporating both mechanisms into a functionalized membrane, an improved control over selectivity can be achieved. We describe the fabrication and experimental characterization of alkali metal cation-selective nanopores in heavy ion-tracked polyimide (PI) membranes using the soft-etched (SE) technique. The latent ion tracks in the PI membrane are selectively dissolved by an organic solvent to form tiny pores without affecting the bulk material. The ionic transport properties of SE-PI membranes are characterized using different electrolyte solutions containing alkali metals, divalent metals, and organic cations under symmetric and asymmetric electrolyte conditions. Under symmetric conditions, the pores exhibit ohmic behavior when exposed to alkali metal chlorides and ammonium chloride solutions while divalent cations cannot pass through the pores as evidenced from the current-voltage curves. For the case of asymmetric electrolyte conditions, current rectification suggests pore blockage from the side of membrane exposed to divalent cations and tetraalkylammonium (TAA) cations. The experimental data show that the SE-PI membranes efficiently discriminate alkali cations from divalent metal cations and ammonium cation from TAA cations. The ionic conduction of the membranes is also sensitive to the mole fraction of Ca^{2+} in multi-ionic solutions. The ionic transport experiments further confirm that the nanopores allow significant alkali cation fluxes while rejecting divalent cations. Based on the good stability and high selectivity, the solvent treated PI membranes constitute remarkable candidates to be employed in applications concerning a wide range of electrolyte solutions.

Keywords: heavy ion irradiation, track-etching, ionic transport, synthetic nanochannels, polymer membranes, nanofluidics

Introduction

Ion channels and biological pores regulate the ionic permeation across the cell membrane allowing communication within the cells, nerve conduction, and signal propagation [1]. Because of their subnanometer diameter and the functional groups lining the channel cavity, they have the ability to selectively pick-up and transport specific ions, while preventing the passage of others [1-3]. Biomimetic membranes exhibiting both chemical and mechanical robustness require the functionalization of pores with diameters in the nanometer and subnanometer range [4, 5]. In the recent decade, synthetic nanoporous membranes have been used in sensing and actuating [6-15], controlled release [16-20], and energy conversion [21-29].

Track-etched polymer membranes show high flexibility and stability under rather demanding conditions. However, chemically track-etched polyethylene terephthalate (PET), polycarbonate (PC), and polyimide (PI) membranes typically show pores with diameters of the order of tens of nanometers which limit their use in the separation of small ions and molecules. To date, several attempts have been made to tune down the pore diameter in order to enhance ionic selectivity. For example, Balme and coworkers have demonstrated the preparation of hybrid biological/artificial solid-state membrane for the selective permeation of alkali ions [30, 31]. The track-etched membranes have been modified by the inclusion of gold nanotubes through electroless deposition technique to reduce the pore diameter [32-34]. The tuning of pore size and surface properties has also been achieved by coating the pore surface with metal oxides using atomic layer deposition (ALD) technique [35-37]. Other nanopores use an atomically thin graphene layer supported on a PET membrane prepared by irradiation with swift heavy ions [38, 39]. Alternatively, the pore diameter can be tuned by grafting stimuli-responsive polymer brushes on the inner pore surface [40-44]. However, pore diameters required to

efficiently discriminate among alkali metal cations or between mono- and divalent metal cations are difficult to achieve.

Recently, Wang and co-workers reported the fabrication of subnanometer pores in heavy ion irradiated PET membrane by using the track-UV technique, thus obtaining high cation selectivity and discrimination between mono- and divalent metal cations [45, 46]. Moreover, Lu *et.al.* demonstrated the fabrication of rectifying channels by growing metal-organic frameworks (MOF) inside PET nanopores and obtained high ionic selectivities [47]. The pores prepared by track-UV or MOF techniques exhibit efficient alkali metal ion transport, showing also high discrimination between mono- and divalent cations.

Among polymers, polyimide (PI) has the ability to maintain its physical, chemical, electrical and mechanical properties over a wide range of temperatures from –269 °C to +400 °C, and is almost insoluble in all organic solvents [48]. Moreover, PI also exhibits high stability toward ion irradiation [49]. Therefore, based on the high chemical, electrical and heat resistance as well as mechanical stability, PI is a good candidate for a heavy ion track membrane in different fields [18, 50]. Despite of its high stability, however, the chemical etching of ion tracks in PI membranes requires harsh conditions compared to the case of the PC and PET membranes and, in particular, it is challenging to obtain membrane pores in the subnanometer-nanometer range.

We describe here the fabrication and characterization of PI membranes irradiated with different heavy ion fluences. In a typical chemical etching of ion tracked PI membrane with NaOCl, covalent bonds are broken by the active chlorine during the channel fabrication process. In this study, we have introduced a unique solvent-assisted nanochannels fabrication in PI membranes. In this technique, the molecular fragments in the damaged ion trails of heavy ions forming the latent tracks are selectively dissolved and extracted out by the organic solvent (EtOH, MeOH, DMF, etc) to form the nanochannels without affecting the bulk material. No

covalent bonds are broken, only van der Waals and hydrogen bonds. This solvent-assisted dissolution of the ion tracks is referred to as the soft-etching (SE) method (see Scheme 1). The ionic conduction behavior of the SE-PI membrane is subsequently studied using aqueous solutions of alkali, divalent metal, and alkylammonium chlorides under symmetric (same solution of both sides) and asymmetric (one side of the membrane is exposed to either KCl or NH_4Cl solution while the other side is exposed to different divalent (M^{2+}) metal chloride or R_4NCl solutions) electrolyte conditions. In the symmetric case, the membranes exhibit ohmic behavior towards alkali solutions, showing high cation-selectivity and transmembrane ionic currents. On the contrary, divalent cations show a drastic current decrease because of nanopore blockage. For the case of asymmetric electrolyte conditions, current rectification and divalent cation blockage is obtained, thus suggesting that the SE-PI membranes can efficiently discriminate between alkali and divalent metal cations. Moreover, they can also discriminate the monovalent organic cations, i.e., ammonium (A^+), tetramethylammonium (TMA^+), tetraethylammonium (TEA^+) and tetrabutylammonium (TBA^+). The ionic conduction under acidic and neutral pH conditions, together with the reduced conduction observed in different metal anion solutions, suggest that the pore surface contains negative charges. Additional permeation experiments further confirm that the nanopores can transfer alkali cations and reject divalent cations.

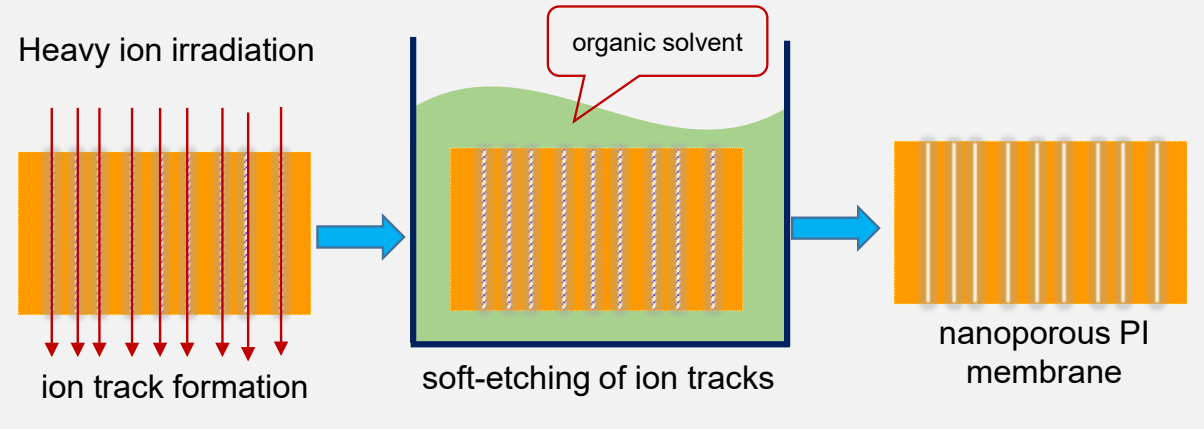

Scheme 1. Scheme representing the nanopore fabrication through soft-etching (SE) technique in a heavy ion-tracked polyimide membrane.

Results and discussion

Ionic selectivity in nanopores (biological or synthetic) is caused either by: (*i*) steric exclusion (only the ions with certain size are allowed to pass through the pore) or by (*ii*) charge exclusion (electrostatic interactions between charged moieties on the inner pore surface and translocating ions). Ionic selectivity control can be achieved by taking into account these parameters. The transport data suggest that the PI membranes obtained with the SE technique (Scheme 1) show effective pore diameters that are close to the combined size of the hydrated alkali metal cations and the native chemical moieties forming the pore charge.

When the irradiated membranes are soaked in organic solvents, the solvent molecules penetrate easily in the ion tracks and selectively dissolve the damaged material, leading to the formation of the nanopores. To facilitate the removal of dissolved material, a voltage of 3 V is applied across the membrane until the current become stable (time ~15 min), as shown in Figures S1(A) and (B). We proceed then to obtain the membrane *I*–*V* characteristics and ionic conductance for the DMF-treated membranes (Figures 1(A)–(D)). These data suggest that DMF can dissolve the damaged material in the ion track throughout the whole membrane length.

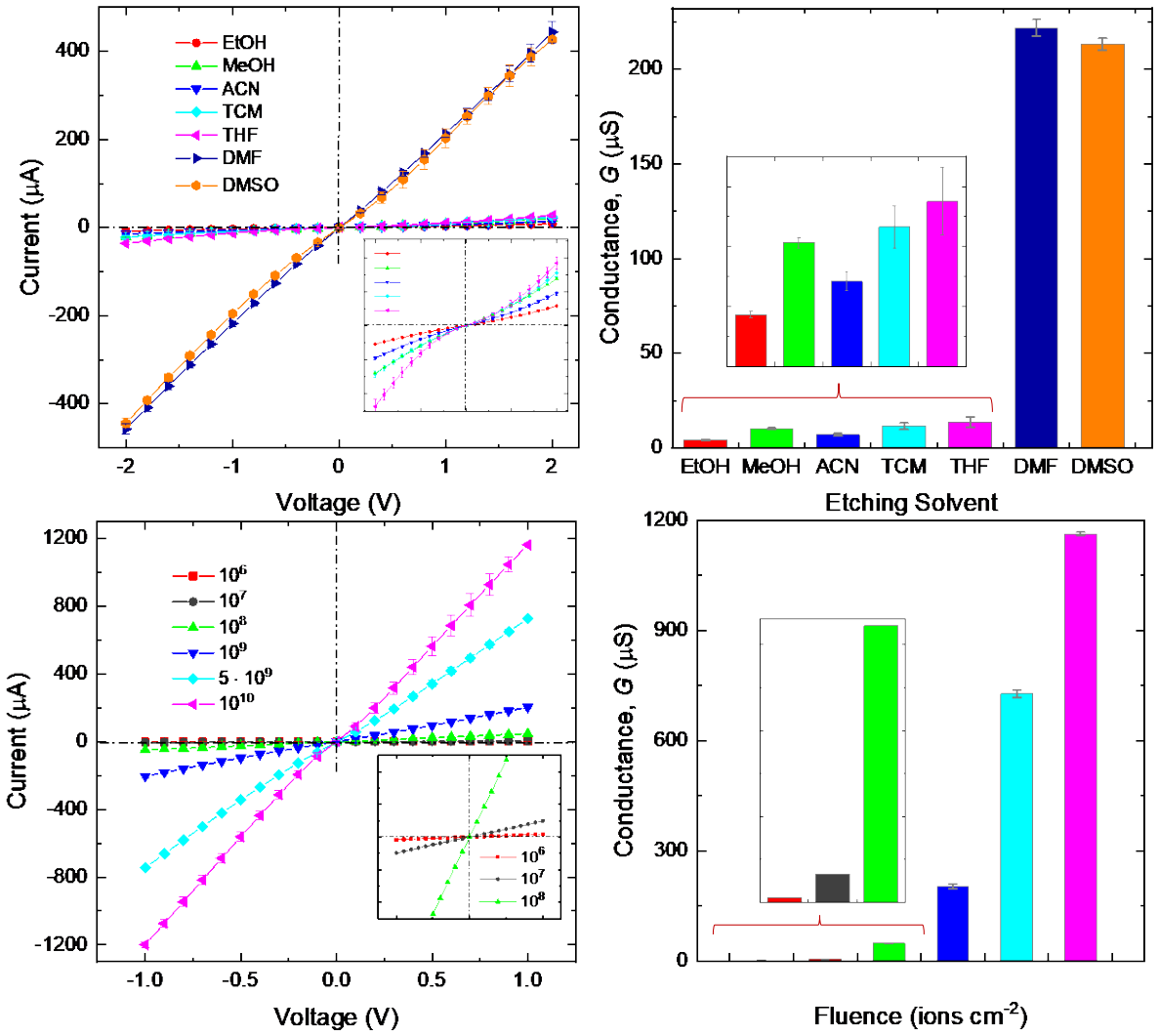

Fig. 1. *I–V* curves (A) and ionic conductances at 2 V (B) for a 100 mM KCl solution in the cases of membranes fabricated using different organic solvents at a fluence 10^9 ions/cm^2. The inset shows the *I–V* curves and conductances for membranes treated with less polar solvents. *I–V* curves (C) and ionic conductances at 1 V (D) for a 100 mM KCl solution in the cases of DMF-treated membranes irradiated with different ion fluences (in ions/cm^2). The inset shows the *I–V* curves and conductances for membranes irradiated with low ion fluences. Note that the PI membranes employed to study the effect of solvent and irradiation fluence are soft-etched for ~ 24 ± 2 hrs at room temperature (~22°C).

Moreover, we have studied the effect of different solvents on the soft-etching of nanopores in the PI membrane. Figures 1(A) and (B) show the *I-V* curves and ion conductances obtained by soaking the membrane in different solvents under the same experimental

conditions. The membranes exposed to DMF and DMSO exhibit much higher conductances than those of the other solvents because their high polarities allow to dissolve and extract efficiently the radiolysis products from the ion tracks. The linear *I–V* behaviour of the membrane soft-etched with DMF and DMSO indicate the symmetric dissolution of ion track to generate cylindrical subnanometer pores Figure 1(A). While, the membranes exposed to other solvent exhibit qausi-linear *I–V* curves (a characteristic of bi-conical shaped pores) shows that the ion track dissolution at the pore opening is higher compared to the interior on the membrane. The DMF based SE technique also allows the fabrication of pores even in the 25 and 50 μm thick membranes. Figures S2(A) and S2(B) show the successive decrease in ion current flow and conductance obtained by increasing the membrane thickness. Note that the imaging of such subnanometer pore under SEM is not possible because of the charging of the membrane surface at low resolution. Therefore, the value of transmembrane ion current and conductances confirmed the formation of tiny pores in PI membrane through soft-etching technique.

We have studied also the effect of ion fluence on the *I-V* curves (Figure 1(C)) and the respective conductances Figure 1(D). In contrast to UV-track technique [45, 46], we have observed a non-linear increase of the ionic conductance with fluence in our SE method. It is likely that irradiation at high fluences leads to overlapping of the latent tracks [18], leading to more damage of polymer chains and radiolysis products in the ion tracks. The membrane polarity is thus enhanced, offering more favourable conditions for the polar solvents to efficiently dissolve the damaged regions, which allows a successful transformation of the latent tracks into nanopores without UV irradiation of the membrane (Figure S2(C)) [45, 46]. Also, the ohmic behavior shown by the linear *I–V* curves suggest the homogeneous dissolution of latent tracks (Figures 1(A) and (C)). The significant increase of ion current with the electrolyte concentration further confirms the formation of nanopores in the PI membrane with SE technique (Figure S2(D)). Moreover, we have also studies the effect of temperature and

exposure time on the dissolution of ion tracks in SE-techniques (Figure S3). The *I–V* data provided in Figure S3 shows that soft-etching of PI membrane at 50°C exhibits drastic increase in the ion current compared to the membrane soft etched for about four weeks at room temperature. This shows that at high temperature the dissolution of ion tracks is much faster than at room temperature using DMF solvent.

We study now the ionic conduction characteristics of the membrane in aqueous electrolyte solution of alkali metal chlorides (LiCl, NaCl, KCl, RbCl and CsCl), divalent metal chlorides ($MgCl_2$, $CaCl_2$, $ZnCl_2$) and ammonium chlorides (NH_4Cl, TMACl, TEACl and TBACl). Figures 2(A)–(F) show the *I–V* curves of membranes treated with MeOH and DMF under symmetric electrolyte conditions. Figures 2(A) and (B) demonstrate that the pores discriminate monovalent cations from divalent cations. While alkali cations are transported across the membrane, the divalent cations show significantly low ionic currents. This fact suggests a comparatively low surface conductance as opposed to bulk ionic conductance and/or a partial blocking due to the presence of a relatively high concentration of divalent ions at the negatively charged pore entrance.[1, 39, 40]

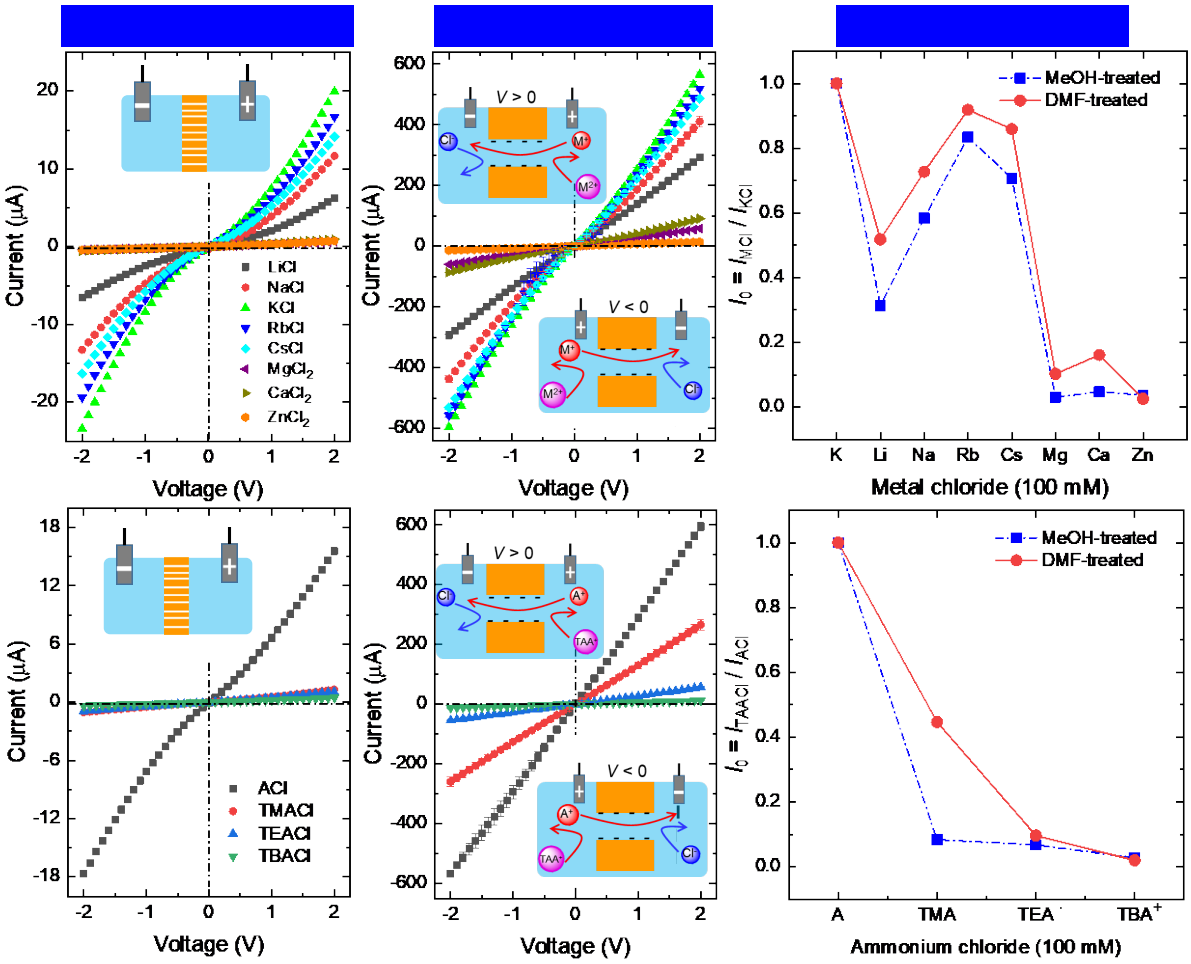

Fig. 2. *I–V* curves and normalized ion currents of MeOH- and DMF-treated membranes for 100 mM alkali and divalent metal chloride solutions (A–C) and 100 mM alkylammonium chloride solutions (D–F) under symmetrical conditions. The inset show schemes of the experimental setup and the ionic transport and rejection processes that occur at positive and negative voltages. Note that the voltage *V* is defined as the potential difference between the right and left solutions.

Figures 2(A) and (B) clearly show that the membrane conductance trend follows the bulk conductivity of alkali metal chloride solutions. On the contrary, the low ionic conductances obtained for all divalent metal chlorides do not correlate with the bulk conductivity (Figure S4) of the solutions confirming further that alkali but not divalent metal cations can permeate through the subnanometer pores. The ionic conduction of the MeOH- and DMF-treated membranes can be compared by defining a normalized ion current I_0 obtained as the ratio of the different metal chloride currents to the KCl current at voltage 2 V. From the I_0 values of

Figure 2(C), we conclude that both MeOH- and DMF-treated membranes exhibit similar conduction characteristics and can discriminate between alkali and divalent cations very efficiently. As expected, the PI membranes obtained by SE method provide high ion currents even at relatively low electrolyte concentrations (100 mM) and voltages (1 V) compared with the case of the UV-track membranes at high concentrations (1M) and voltages (10 V) [45, 46].

We have also analyzed the transport of organic ammonium cations in Figures 2(D)–(F). The membranes conduct ammonium (A^+) similarly to potassium (K^+) because of their almost identical ionic conductivities and diffusion coefficients. Among all the organic cations studied here, A^+ exhibits the highest ion current while a significant current decrease is noticed on replacing the hydrogen atoms of central nitrogen atom in ammonium with alkyl (methyl, ethyl and butyl) moieties. For the case of DMF-treated membrane, the highest current corresponds to A^+ to because of its relatively small size and lower hydrophobicity compared with those of TMA^+, TEA^+ and TBA^+ [51]. As expected, the ion current and conductance decrease in the order $A^+ > TMA^+ > TEA^+ >> TBA^+$. For the case of MeOH-treated membrane, however, a significant decrease in the current was observed even for the TMACl solution, suggesting the blockage of pores. This shows that the effective pore diameter of the MeOH-treated membrane is smaller than that the DMF-treated ones, as suggested also by Figures 2(A)–(C). In the case of Figures 2(D)–(F), the current decreases should be attributed to the effects of cation size and solvation, as well as to the partial blockage due to the adsorption of the bulky organic cations on the pore entrance. Thus, the PI membranes obtained by soft-etched technique can discriminate not only between alkali cations and divalent cations but also between organic cations of different size and hydrophobicity. Other data showing the changes in the ionic conductance of the MeOH- and DMF-treated membranes with respect to the bulk conductivity of ammonium chloride are shown in Figure S5. On the other hand, for the PI membrane prepared by traditional chemical track-etching technique (NaOCl as an etchant) the obtained

transmembrane ionic currents and conductances of alkali, divalent and alkylammonium chlorides are correlated with the bulk conductivity of the solutions which shows that all the metals and organic cations can flow across the membrane (Figure S6).

Figures 3(A)–(F) show the behavior of SE-PI membranes under asymmetrical electrolyte conditions. Here, one side of the membrane is exposed to the KCl or NH_4Cl solutions while the other side is in contact with different metal or ammonium chloride solutions. The current rectification observed under asymmetric conditions (Figures 3(A)–(C)) suggests that high currents are obtained when the monovalent cations are forced to the pore ($V > 0$, monovalent pore mode) while low currents correspond to forcing the divalent cations ($V < 0$, divalent pore mode), Figures 3(A) and (B). For the case of Figures 3(D)–(F), the ammonium ions can pass through pore leading to high currents at $V > 0$. On the contrary, the bulky cations cannot pass through the pore at $V < 0$ which leads to current rectification. Figure 3(F) clearly shows an increase in the rectification with the ammonium cation size.

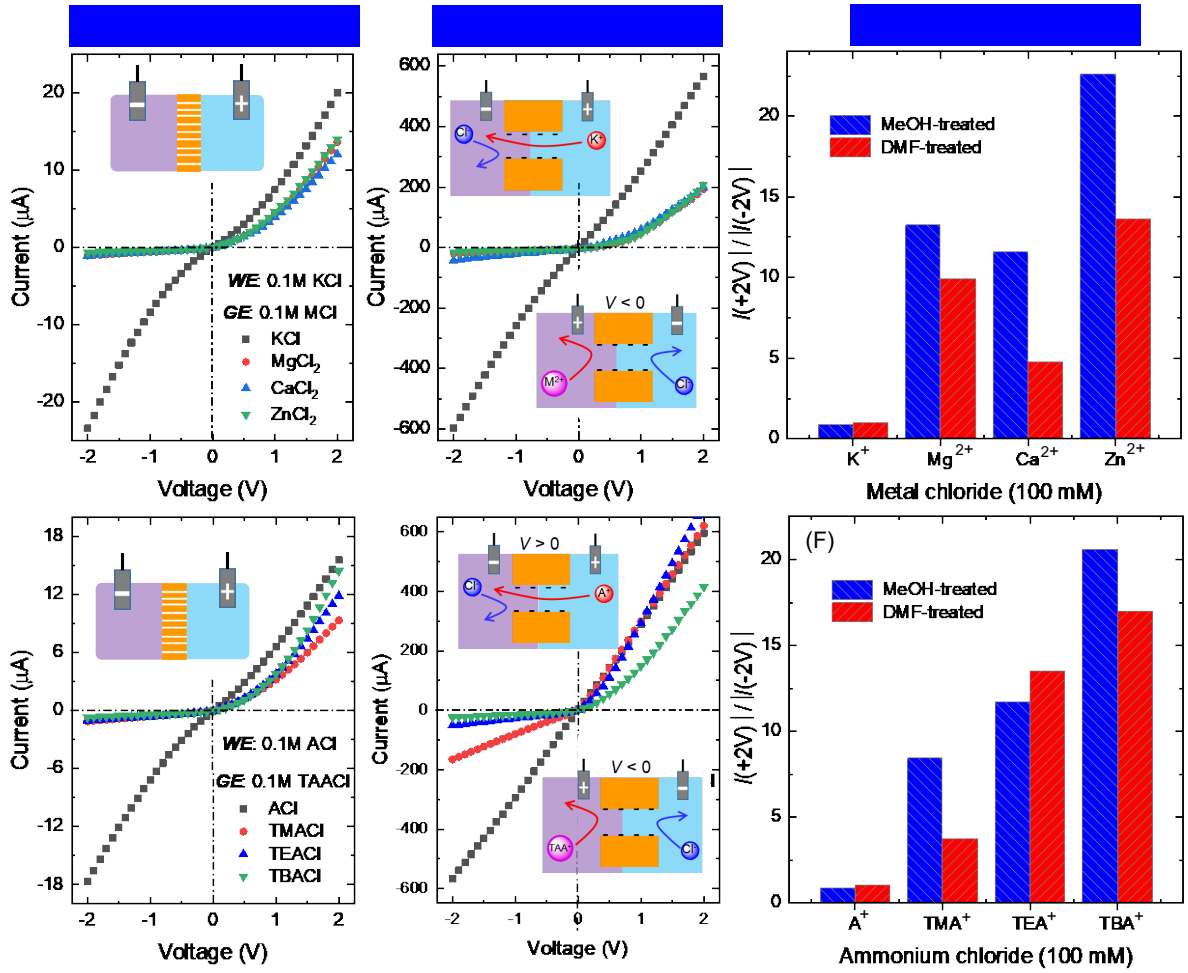

Fig. 3. *I–V* curves of MeOH- (A) and DMF (B) -treated membranes in metal chloride solutions under asymmetrical conditions. One side of the membrane (working electrode, WE) is exposed to a 100 mM KCl solution while the other side (ground electrode, GE) is exposed to 100 mM different divalent (M^{2+}) metal chloride solutions. Rectification of the MeOH- and DMF-treated membranes in metal chloride solutions (C). *I–V* curves of MeOH- (D) and DMF (E) -treated membranes in alkyl ammonium chloride solutions under asymmetrical conditions. One side of the membrane is exposed to a 100 mM NH_4Cl solution while the other side is exposed to 100 mM different alkylammonium chloride solutions. Rectification of the MeOH- and DMF-treated membrane in alkylammonium chloride solutions (F). The insets show schemes of the experimental setup and the ionic transport and rejection at positive and negative voltages.

To better show the effects of the electrostatic interaction and size of metal cations, we have also considered the case of neutral and acidic conditions (Figure 4(A)). PI nanopores are negatively charged due to the presence of functional moieties on the pore surface that are

generated during the chemical track-etching process [52, 53]. In the case of membranes obtained by soft-etch technique, the pores are also negatively charged and the accumulation of divalent cations at the pore entrance causes a partial blocking in the nanopore. Under acidic conditions, however, the pore surface becomes neutral and cannot interact electrically with the metal cations. Figure 4(A) shows the pH-dependent ionic conductance of solvent treated membranes obtained from the corresponding *I-V* curves of Figures S7(A) and (B). For the case of alkali cations, the conductance is decreased at acidic compared with neutral conditions due to the loss of cation-selectivity in the uncharged pore. On the contrary, a slight increase in the ionic conductance is noticed in acidic solutions of divalent metal cations compared with the case of neutral conditions. This suggest a negligible electrostatic interaction between divalent cations and pores. Figure 4(A) also shows that neutral pores still discriminate the alkali from divalent cations even under acidic conditions, suggesting again a nanoscale pore diameter.

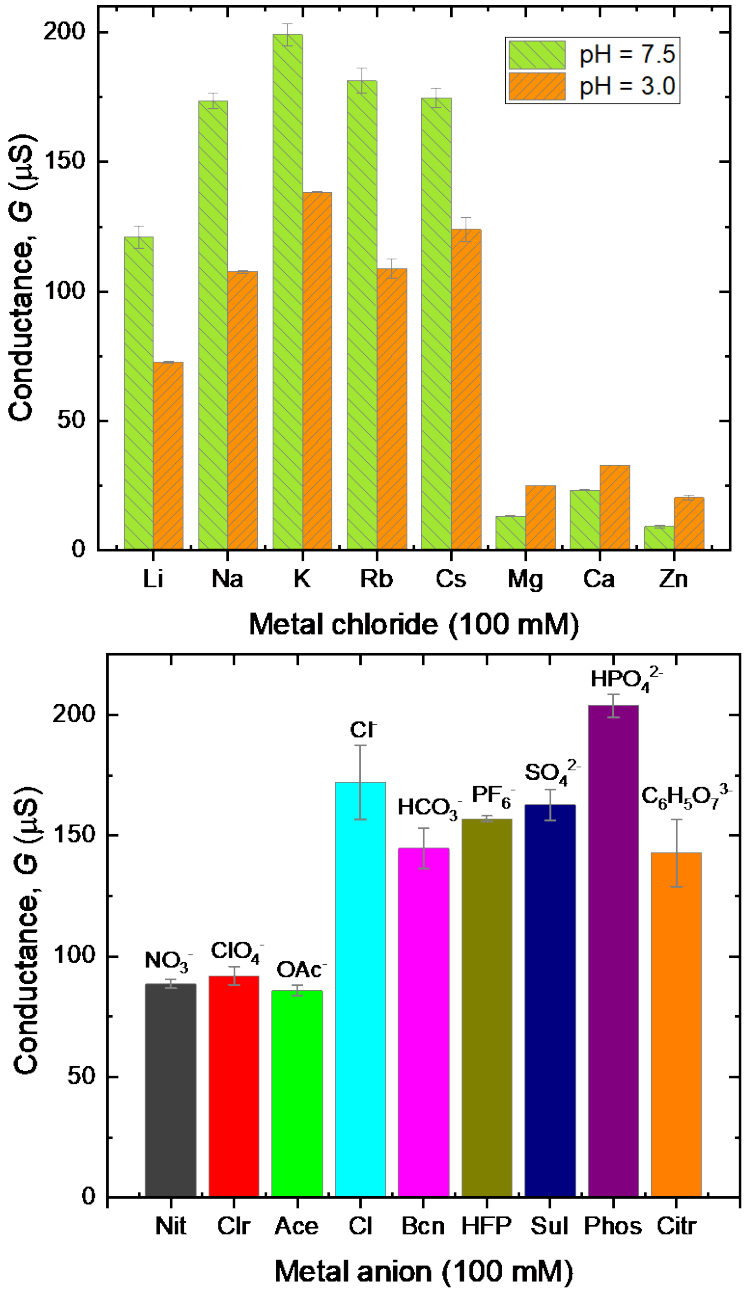

Fig. 4 Ionic conductance of DMF-treated membranes in 100 mM metal chloride solutions at 2 V under close to neutral and acidic conditions (A). Ionic conductance of DMF-treated membranes in aqueous electrolyte solutions with different anions at 2 V (B).

The ionic conductances of different anions in the DMF-treated membranes shown in Figure 4(B) are obtained from the respective *I–V* curves of Figure S7(C). In this experiment, sodium salts with the anions nitrate (NO_3^-), chlorate (ClO_4^-), acetate (OAc^-), and potassium

salts of chloride (Cl^-), bicarbonate (HCO_3^-), hexafluorophosphate (PF_6^-), sulfate (SO_4^{2-}), hydrogen phosphate (HPO_4^{2-}), and citrate ($C_6H_5O_7^{3-}$) are prepared in water at physiological pH conditions. Figure 4(B) shows that the membrane conductance series for the different electrolytes correlate with their bulk conductivity values shown in Figure S7(D) except for the case of trivalent citrate anion. In general, the anions are excluded from the negatively charged pores and do not interfere with the transport of cations, confirming again the cation-selective behavior of SE-PI membranes.

Because of the relevant role of the calcium and potassium cations in biological [46] and artificial pores [46], we consider now multi-ionic systems in the SE-membranes. Figures 5(A)–(F) show the *I–V* curves and the normalized ionic conductance G_0 in electrolyte solutions with different mole fractions (X_{Ca}) of Ca^{2+} under symmetric and asymmetric conditions. By increasing X_{Ca}, the membrane is converted from the monovalent to the divalent cation form at both $V > 0$ and $V < 0$ for symmetric conditions (Figures 5(A)–(C) and S8). Note the abrupt decrease of the membrane currents with X_{Ca}, in contrast with the increase of the bulk conductivity with X_{Ca} shown in Figures S8(A)–(D) [46]. First, the surface conductance of the divalent ions [46] should be lower than that of the monovalent ions [54] because of the strong interaction with the negatively charged groups on the pore surface which may also give local charge inversion phenomena [55]. Second, an effective electrostatic blocking due to the accumulation of divalent cations at the negative pore entrance can slow down the ions access and progression through the membrane. These effects have been qualitatively accounted for in Figure 5(C) by fitting the experimental data to the phenomenological equation $G = G_0/(1 + KX_{Ca})$ where G_0 is the reference conductance measured at $X_{Ca} = 0$ and K is an empirical constant. The small difference between the two curves obtained at positive and negative voltages probably reflects an inherent asymmetry of the presumed cylindrical pore.

For the case of asymmetric conditions (Figures 5(D)–(F) and S9), the observed current rectification suggests that high currents correspond to forcing the potassium cations to the pore ($V > 0$, monovalent pore mode) while low currents correspond to forcing the calcium cations to the pore ($V < 0$, divalent pore mode), in agreement with Figures 3(A) and (B). Figure 5(F) shows that the currents obtained in Figures 5(D) and (E) for the monovalent pore mode ($V > 0$) do not depend on the X_{Ca} value in clear contrast with the divalent pore mode ($V < 0$). Note that the fitting of the experimental data to the same phenomenological equation used in Figure 5(C) permits the determination of the unique parameter (K) introduced in Figure 5(F), which is of the order of 10 for most of the measured G vs. X_{Ca} curves. This empirical constant constitutes a measure of the strong interaction of the divalent cations with the pore charge groups and suggests that the accumulation of divalent cations at the negative pore entrance can slow down the access and progression through the membrane.

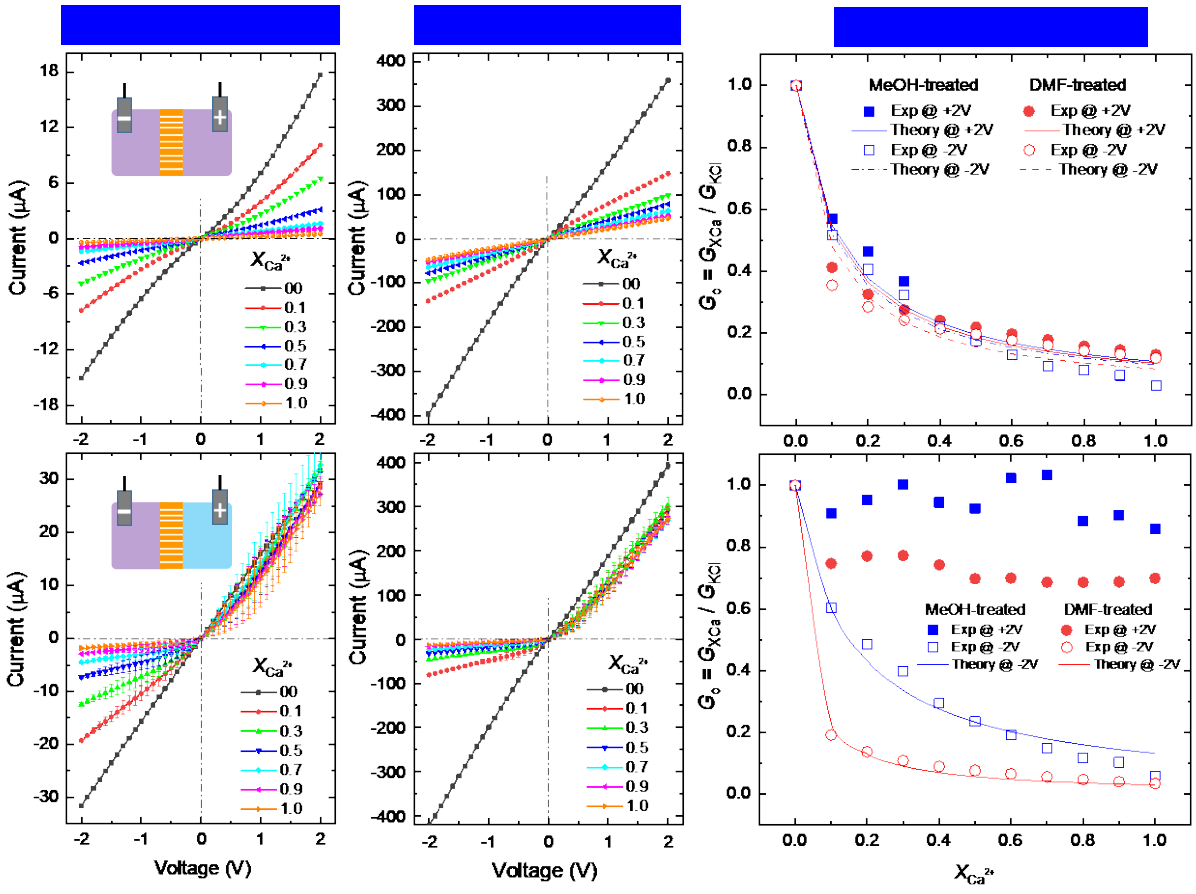

Fig. 5. *I–V* curves and KCl-normalized conductance of MeOH- and DMF-treated membranes at different Ca^{2+} mole fractions with [KCl + $CaCl_2$] = 100 mM under symmetric (A–C) and asymmetric (D–F) electrolyte conditions.

To investigate further the ion selectivity of the SE-membranes to alkali and divalent metal cations, we have also conducted the transport experiments. The experimental data shows that SE-PI membrane are not able to differentiate in between alkali cations, i.e., they can freely permeate across the membrane. Therefore, for permeation experiment only KCl is used to investigate the monovalent ion selectivity and discrimination ability of the membrane towards divalent cations. To this end, the membrane separates the metal chloride feed solution (1 M) from the deionized water permeate solution. In this case, the transport of ions occurs because of the concentration gradient without applying any external field. The ionic permeation is monitored by the concentration increase in the permeate solution which is obtained from the electrical conductivity at prescribed time periods (Figure 6(A)). In the case of KCl, the permeate solution conductivity increases rapidly compared with those of the divalent metal chloride solutions, showing again that these pores conduct K^+ ions efficiently and reject divalent metal cations. A measure of the monovalent/divalent selectivity is the KCl salt flux scaled to the $CaCl_2$, $MgCl_2$, and $ZnCl_2$ salt fluxes (Figure 6(B)). These ratios are obtained from the slope of the conductivity versus time experimental data (Figure 6(A)) and show again a significant selectivity towards the cation charge number.

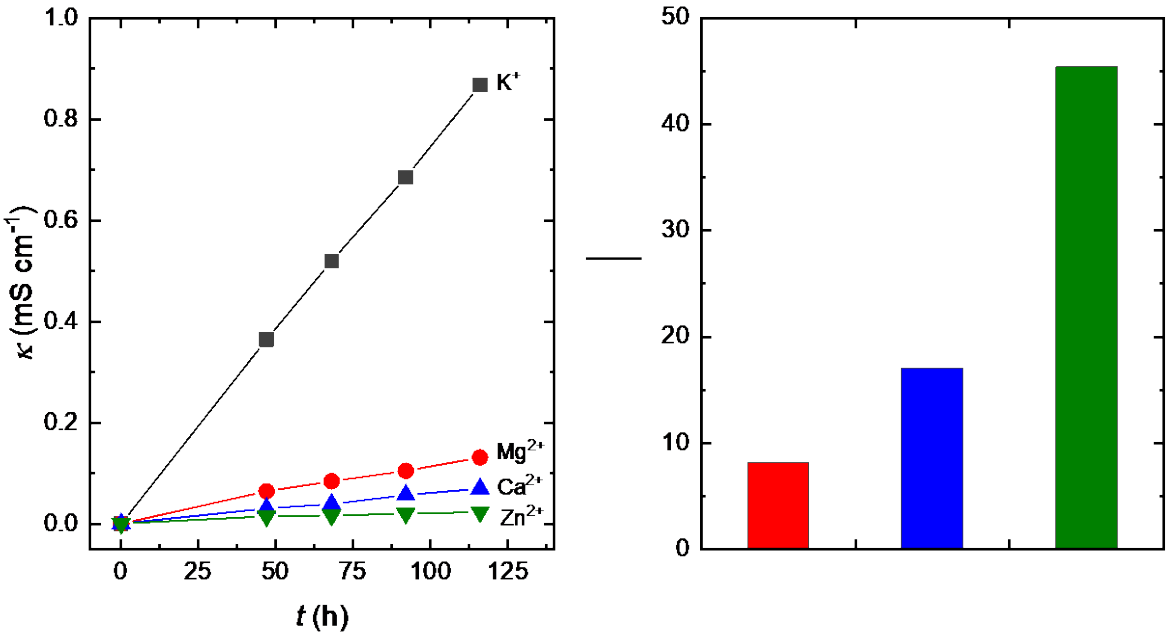

Fig. 6. Permeate conductivity versus time as a measure of metal cation transport from a feed 1 M metal chloride solution through a DMF-treated membrane (A) and the resulting KCl salt flux scaled to the $CaCl_2$, $MgCl_2$, and $ZnCl_2$ salt fluxes, J_{KCl}/J_{MCl_2}, where M denotes the divalent cation (B). This ratio of experimental fluxes is a measure of the monovalent/divalent selectivity. It can be obtained from the slope of the conductivity versus time lines assuming a linear relationship between ionic conductivity and concentration, which includes an approximately constant factor involving the ionic diffusion coefficients and charge numbers.[1,48]

Conclusions

We have demonstrated that soft-etched PI membranes show an efficient (high currents and permeation rates) and selective (significant monovalent/divalent discrimination) transport of alkali ions. The ionic transport properties of SE-PI membranes have been studied with different electrolyte solutions containing alkali metal, divalent metal, and organic cations under symmetric and asymmetric electrolyte conditions. Under symmetric conditions, the nanopores show ohmic behavior for alkali metal chlorides and ammonium chloride solutions while divalent cations cannot pass through, as evidenced from the drastic drops of transmembrane ion currents. On the contrary, significant ion current rectification is obtained under asymmetric

conditions. The *I–V* curves of the PI membranes obtained by soft-etched technique show clear differences between alkali cations as well as between organic cations, discriminating also between monovalent divalent metal cations. In addition, the ionic conduction of the membranes is very sensitive to the mole fraction of Ca^{2+} in a multi-ionic electrolyte solution, thus providing electrostatic and steric insights on potassium and calcium selectivity in biological systems. The transport experiment proves that alkali cations but not divalent cations can efficiently permeate the membrane.

Based on the good stability and high discrimination capability, we envision that the SE-PI membrane fabricated and characterized here should be useful in different applications with electrolyte solutions and mixtures [56]. Moreover, the selectivity, sensitivity, and fast electrical response of these membranes could also be used to miniaturize sensing devices for the detection of different analytes in biological fluids.

Materials and methods

Chemicals: All the chemicals and solvents used in the study are purchased from Sigma-Aldrich, Schnelldorf, Germany, and used without further purification. The chemicals include ammonium chloride (NH_4Cl, ≥99.5%), tetramethylammonium chloride (TMACl, ≥98.0%), tetraethylammonium chloride (TEACl, ≥98%), tetrabutylammonium chloride (TBACl, ≥97.0%), lithium chloride (LiCl, ≥99.0%), sodium chloride, (NaCl, ≥99.9%), potassium chloride (KCl, ≥99.0%), rubidium chloride (RbCl, 99.8%) and cesium chloride (CsCl, 99.9%), magnesium chloride ($MgCl_2$, ≥99.0%), calcium chloride ($CaCl_2$, 93.0%), zinc chloride ($ZnCl_2$, ≥98%), sodium nitrate ($NaNO_3$, ≥99%), sodium chlorate ($NaClO_4$, ≥98.0%), sodium acetate (NaOAc, ≥99.0%), potassium bicarbonate ($KHCO_3$, ≥99.5%), potassium hexafluorophosphate (KPF_6, ≥99%), potassium sulphate (K_2SO_4, ≥99.0%), potassium phosphate dibasic (K_2HPO_4, ≥98%) and potassium citrate tribasic ($K_3C_6H_5O_7$, ≥99.0%). The solvents are methanol (MeOH, 99.8%), ethanol (EtOH, 99.8%), acetonitrile (ACN), trichloromethane (TCM, 99.5%e),

tetrahydrofuran (THF, ≥99.9%), dimethylformamide (DMF, 99.8%) and dimethylsulfoxide (DMSO, ≥99.9%).

Fabrication of nanoporous membrane: The PI membranes (Kapton50 HN, DuPont; 12 μm thick) are irradiated with swift heavy ions (Au) of energy 11.4 MeV per nucleon at the linear accelerator UNILAC (GSI Helmholtzzentrum für Schwerionenforschung, Darmstadt, Germany). The membranes used are irradiated with ion fluences in the range 10^6 – 10^{10} ions/cm^2. The ion tracks are activated by exposing the irradiated membranes to UV light (320 nm) on both sides for 1 hr. Subsequently, the ion-tracked membranes are immersed in an organic solvent (Scheme 1) for at least 24 h at room temperature and washed with distilled water before measurements.

Current–voltage (I–V) curves. The membrane is fixed in between two chambers of a home-made electrochemical cell to characterize the electrical response [21, 57]. The cell chambers are made of polychlorotrifluoroethylene (PCTFE), also known as Neoflon. Each chamber contains a circular hole of ~8 mm^2 in diameter which constitutes the effective membrane area exposed. A maximum solution volume of ~1.5 mL can be filled in each chamber. Prior to the measurements, the remaining damaged material is removed from the membrane by applying a potential difference (voltage) in the form of rectangle wave signal using Au-electrodes until the current becomes stable. For the *I-V* measurements, Ag|AgCl electrodes are immersed into the electrolyte solutions on both membrane sides to control the input potentials and output currents [21, 57]. The input potential, a triangular wave signal, gives the resulting current which is recorded with a Keithley 6487 picoammeter (Keithley Instruments, Cleveland, Ohio) [21, 57].

Ion Transport experiment: Metal ion transport across the membrane with 10^9 pores/cm^2 is also studied using a two-compartment cell. The maximum volume of each chamber is ~5.0 mL with an effective permeation membrane area of ~8 mm^2. To this end, the membrane sample

is fixed in between the feed and permeate compartments. The feed compartment is filled with a 1 M aqueous solution of either a monovalent or a divalent chloride and the permeate compartment contains deionized water only. The solutions of both compartments are continuously stirred and the time-dependent concentration of ions in the permeate chamber is monitored by measuring the bulk conductivity of the permeate solution with a conductivity meter (Cond 315i /SET from WTW).

Supporting Information

The Supporting Information is available free of charge on the ACS Publications website at DOI:

Acknowledgements

P.R., J. C., and S. M. acknowledge the funding from project PGC2018-097359-B-I00, Spanish Ministry of Science and Education, and FEDER. K.F., M.A., S.N. and W.E. acknowledge the support from the LOEWE project iNAPO, Hessen State Ministry of Higher Education, Research and the Arts, Germany. The authors are thankful to Prof. C. Trautmann and Dr. E. Toimil Molares (GSI, Material Research Department) for their support with the heavy ion irradiation experiments and Mr. E. Schubert for the designing of electrochemical cells. The heavy ion irradiation is based on a UMAT experiment, which was performed at the X0-beamline of the UNILAC at the GSI Helmholtzzentrum fuer Schwerionenforschung, Darmstadt (Germany) in the frame of FAIR Phase-0.

Notes and references

[1] B. Hille, Ionic channels of excitable membranes, 3rd ed., Sinauer Associates Inc., Sunderland, MA, 2001.
[2] S.W. Kowalczyk, T.R. Blosser, C. Dekker, Biomimetic nanopores: learning from and about nature, Trends Biotechnol., 29 (2011) 607-614.
[3] M. Barboiu, A. Gilles, From Natural to Bioassisted and Biomimetic Artificial Water Channel Systems, Acc. Chem. Res., 46 (2013) 2814-2823.
[4] T. Ma, J.-M. Janot, S. Balme, Track-Etched Nanopore/Membrane: From Fundamental to Applications, Small Methods, 2000366. (2020) https://doi.org/10.1002/smtd.202000366.
[5] X. Hou, Smart Gating Multi-Scale Pore/Channel-Based Membranes, Adv. Mater., 28 (2016) 7049-7064.
[6] M. Ali, R. Neumann, W. Ensinger, Sequence-Specific Recognition of DNA Oligomer Using Peptide Nucleic Acid (PNA)-Modified Synthetic Ion Channels: PNA/DNA Hybridization in Nanoconfined Environment, ACS Nano, 4 (2010) 7267-7274.
[7] M. Ali, P. Ramirez, I. Duznovic, S. Nasir, S. Mafe, W. Ensinger, Label-free histamine detection with nanofluidic diodes through metal ion displacement mechanism, Colloids Surf., B, 150 (2017) 201-208.
[8] M. Ali, M.N. Tahir, Z. Siwy, R. Neumann, W. Tremel, W. Ensinger, Hydrogen Peroxide Sensing with Horseradish Peroxidase-Modified Polymer Single Conical Nanochannels, Anal. Chem., 83 (2011) 1673-1680.
[9] H. Bayley, P.S. Cremer, Stochastic sensors inspired by biology, Nature, 413 (2001) 226-230.
[10] K. Healy, B. Schiedt, A.P. Morrison, Solid-state nanopore technologies for nanopore-based DNA analysis, Nanomedicine, 2 (2007) 875-897.
[11] A. de la Escosura-Muñiz, A. Merkoçi, Nanochannels Preparation and Application in Biosensing, ACS Nano, 6 (2012) 7556-7583.
[12] S. Nasir, M. Ali, I. Ahmed, C.M. Niemeyer, W. Ensinger, Phosphoprotein Detection with a Single Nanofluidic Diode Decorated with Zinc Chelates, ChemPlusChem, 85 (2020) 587-594.
[13] Y. Zhao, J.-M. Janot, E. Balanzat, S. Balme, Mimicking pH-Gated Ionic Channels by Polyelectrolyte Complex Confinement Inside a Single Nanopore, Langmuir, 33 (2017) 3484-3490.
[14] K. Zhan, Z. Li, J. Chen, Y. Hou, J. Zhang, R. Sun, Z. Bu, L. Wang, M. Wang, X. Chen, X. Hou, Tannic acid modified single nanopore with multivalent metal ions recognition and ultra-trace level detection, Nano Today, 33 (2020) 100868.
[15] X. Zhang, F. Zhang, F. Zhu, X. Zhang, D. Tian, R.P. Johnson, H. Li, Bioinspired γ-Cyclodextrin Pseudorotaxane Assembly Nanochannel for Selective Amino Acid Transport, ACS Appl. Bio Mater., 2 (2019) 3607-3612.
[16] R. Duan, F. Xia, L. Jiang, Constructing Tunable Nanopores and Their Application in Drug Delivery, ACS Nano, 7 (2013) 8344-8349.
[17] L.E. Ermakova, M.P. Sidorova, M.E. Bezrukova, Filtration and electrokinetic characteristics of track membranes, Colloid J. (USSR), 60 (1998) 705-712.
[18] R.L. Fleischer, P.B. Price, R.M. Walker., Nuclear tracks in Solids: Principles and Applications, Berkeley: University of California Press1975.
[19] X. Hou, W. Guo, L. Jiang, Biomimetic smart nanopores and nanochannels, Chem. Soc. Rev., 40 (2011) 2385-2401.
[20] W.T.S. Huck, Responsive polymers for nanoscale actuation, Mater. Today, 11 (2008) 24-32.

[21] P. Ramirez, J. Cervera, V. Gomez, M. Ali, S. Nasir, W. Ensinger, S. Mafe, Optimizing Energy Transduction of Fluctuating Signals with Nanofluidic Diodes and Load Capacitors, Small, 14 (2018).
[22] P. Ramirez, V. Gomez, J. Cervera, S. Nasir, M. Ali, W. Ensinger, S. Mafe, Energy conversion from external fluctuating signals based on asymmetric nanopores, Nano Energy, 16 (2015) 375-382.
[23] Y.P. Feng, W.W. Zhu, W. Guo, L. Jiang, Bioinspired Energy Conversion in Nanofluidics: A Paradigm of Material Evolution, Adv. Mater., 29 (2017).
[24] K. Xiao, P. Giusto, L.P. Wen, L. Jiang, M. Antonietti, Nanofluidic Ion Transport and Energy Conversion through Ultrathin Free-Standing Polymeric Carbon Nitride Membranes, Angew. Chem. Int. Ed., 57 (2018) 10123-10126.
[25] G. Laucirica, A.G. Albesa, M.E. Toimil-Molares, C. Trautmann, W.A. Marmisollé, O. Azzaroni, Shape matters: Enhanced osmotic energy harvesting in bullet-shaped nanochannels, Nano Energy, 71 (2020) 104612.
[26] J. Kim, S.J. Kim, D.-K. Kim, Energy harvesting from salinity gradient by reverse electrodialysis with anodic alumina nanopores, Energy, 51 (2013) 413-421.
[27] S. Balme, T. Ma, E. Balanzat, J.-M. Janot, Large osmotic energy harvesting from functionalized conical nanopore suitable for membrane applications, J. Membr. Sci., 544 (2017) 18-24.
[28] Y. Zhu, K. Zhan, X. Hou, Interface Design of Nanochannels for Energy Utilization, ACS Nano, 12 (2018) 908-911.
[29] J. Zhang, K. Zhan, S. Wang, X. Hou, Soft interface design for electrokinetic energy conversion, Soft Matter, 16 (2020) 2915-2927.
[30] S. Balme, J.M. Janot, L. Berardo, F. Henn, D. Bonhenry, S. Kraszewski, F. Picaud, C. Ramseyer, New Bioinspired Membrane Made of a Biological Ion Channel Confined into the Cylindrical Nanopore of a Solid-State Polymer, Nano Lett., 11 (2011) 712-716.
[31] S. Balme, F. Picaud, S. Kraszewski, P. Déjardin, J.M. Janot, M. Lepoitevin, J. Capomanes, C. Ramseyer, F. Henn, Controlling potassium selectivity and proton blocking in a hybrid biological/solid-state polymer nanoporous membrane, Nanoscale, 5 (2013) 3961-3968.
[32] C.R. Martin, M. Nishizawa, K. Jirage, M.S. Kang, S.B. Lee, Controlling ion-transport selectivity in gold nanotubule membranes, Adv. Mater., 13 (2001) 1351-1362.
[33] C.R. Martin, Z. Siwy, Molecular filters - Pores within pores, Nat. Mater., 3 (2004) 284-285.
[34] K.B. Jirage, J.C. Hulteen, C.R. Martin, Nanotubule-based molecular-filtration membranes, Science, 278 (1997) 655-658.
[35] A. Spende, N. Sobel, M. Lukas, R. Zierold, J.C. Riedl, L. Gura, I. Schubert, J.M.M. Moreno, K. Nielsch, B. Stühn, C. Hess, C. Trautmann, M.E. Toimil-Molares, TiO2, SiO2, and Al2O3coated nanopores and nanotubes produced by ALD in etched ion-track membranes for transport measurements, Nanotechnology, 26 (2015) 335301.
[36] P. Chen, T. Mitsui, D.B. Farmer, J. Golovchenko, R.G. Gordon, D. Branton, Atomic Layer Deposition to Fine-Tune the Surface Properties and Diameters of Fabricated Nanopores, Nano Lett., 4 (2004) 1333-1337.
[37] C.-M. Wang, D.-L. Kong, Q. Chen, J.-M. Xue, Surface engineering of synthetic nanopores by atomic layer deposition and their applications, Front. Mater. Sci., 7 (2013) 335-349.
[38] Y. Fu, X. Guo, Y. Wang, X. Wang, J. Xue, An atomically-thin graphene reverse electrodialysis system for efficient energy harvesting from salinity gradient, Nano Energy, 57 (2019) 783-790.
[39] W. Li, L. Liang, S. Zhao, S. Zhang, J. Xue, Fabrication of nanopores in a graphene sheet with heavy ions: A molecular dynamics study, J. Appl. Phys., 114 (2013) 234304.

[40] W. Guo, H.W. Xia, L.X. Cao, F. Xia, S.T. Wang, G.Z. Zhang, Y.L. Song, Y.G. Wang, L. Jiang, D.B. Zhu, Integrating Ionic Gate and Rectifier Within One Solid-State Nanopore via Modification with Dual-Responsive Copolymer Brushes, Adv. Funct. Mater., 20 (2010) 3561-3567.
[41] S. Nasir, M. Ali, W. Ensinger, Thermally controlled permeation of ionic molecules through synthetic nanopores functionalized with amine-terminated polymer brushes, Nanotechnology, 23 (2012) 225502.
[42] G. Pérez-Mitta, J.S. Tuninetti, W. Knoll, C. Trautmann, M.E. Toimil-Molares, O. Azzaroni, Polydopamine Meets Solid-State Nanopores: A Bioinspired Integrative Surface Chemistry Approach To Tailor the Functional Properties of Nanofluidic Diodes, J. Am. Chem. Soc., 137 (2015) 6011-6017.
[43] M. Tagliazucchi, I. Szleifer, Stimuli-responsive polymers grafted to nanopores and other nano-curved surfaces: structure, chemical equilibrium and transport, Soft Matter, 8 (2012) 7292-7305.
[44] B. Yameen, M. Ali, R. Neumann, W. Ensinger, W. Knoll, O. Azzaroni, Synthetic Proton-Gated Ion Channels via Single Solid-State Nanochannels Modified with Responsive Polymer Brushes, Nano Lett., 9 (2009) 2788-2793.
[45] Q. Wen, D. Yan, F. Liu, M. Wang, Y. Ling, P. Wang, P. Kluth, D. Schauries, C. Trautmann, P. Apel, W. Guo, G. Xiao, J. Liu, J. Xue, Y. Wang, Highly Selective Ionic Transport through Subnanometer Pores in Polymer Films, Adv. Funct. Mater., 26 (2016) 5796-5803.
[46] P. Wang, M. Wang, F. Liu, S. Ding, X. Wang, G. Du, J. Liu, P. Apel, P. Kluth, C. Trautmann, Y. Wang, Ultrafast ion sieving using nanoporous polymeric membranes, Nat. Commun., 9 (2018) 569.
[47] J. Lu, H. Zhang, J. Hou, X. Li, X. Hu, Y. Hu, C.D. Easton, Q. Li, C. Sun, A.W. Thornton, M.R. Hill, X. Zhang, G. Jiang, J.Z. Liu, A.J. Hill, B.D. Freeman, L. Jiang, H. Wang, Efficient metal ion sieving in rectifying subnanochannels enabled by metal–organic frameworks, Nat. Mater., (2020).
[48] M.K. Ghosh, k.L. Mittal, Polyimides: fundamentals and applications, Marcel Dekker, Inc, New York, 1996.
[49] H. Inoue, H. Okamoto, Y. Hiraoka, Effect of the chemical structure of acid dianhydride in the skeleton on the thermal property and radiation resistance of polyimide, Radiat. Phys. Chem., 29 (1987) 283-288.
[50] C. Trautmann, S. Bouffard, R. Spohr, Etching threshold for ion tracks in polyimide, Nucl. Instrum. Methods Phys. Res., Sect. B, (1996) 429-433.
[51] Y. Koga, P. Westh, K. Nishikawa, S. Subramanian, Is a Methyl Group Always Hydrophobic? Hydrophilicity of Trimethylamine-N-oxide, Tetramethyl Urea and Tetramethylammonium Ion, J. Phys. Chem. B, 115 (2011) 2995-3002.
[52] M. Ali, B. Schiedt, K. Healy, R. Neumann, W. Ensinger, Modifying the surface charge of single track-etched conical nanopores in polyimide, Nanotechnology, 19 (2008) 085713.
[53] Z. Siwy, D. Dobrev, R. Neumann, C. Trautmann, K. Voss, Electro-responsive asymmetric nanopores in polyimide with stable ion-current signal, Appl. Phys., 76 (2003) 781-785.
[54] S. Mafé, J.A. Manzanares, P. Ramirez, Modeling of surface vs. bulk ionic conductivity in fixed charge membranes, Phys. Chem. Chem. Phys., 5 (2003) 376-383.
[55] K. Lin, C.-Y. Lin, J.W. Polster, Y. Chen, Z.S. Siwy, Charge Inversion and Calcium Gating in Mixtures of Ions in Nanopores, J. Am. Chem. Soc., 142 (2020) 2925-2934.
[56] T. Luo, S. Abdu, M. Wessling, Selectivity of ion exchange membranes: A review, J. Membr. Sci., 555 (2018) 429-454.
[57] P. Ramirez, V. Garcia-Morales, V. Gomez, M. Ali, S. Nasir, W. Ensinger, S. Mafe, Hybrid Circuits with Nanofluidic Diodes and Load Capacitors, Phys. Rev. Applied, 7 (2017).

TOC Graphics

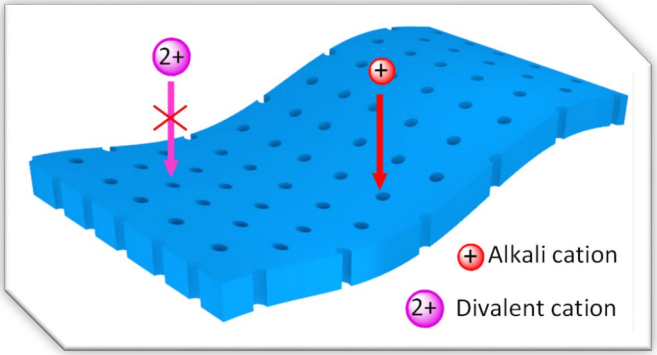

Supporting Information

Fabrication of Soft-Etched Nanoporous Polyimide Membranes for Ionic Conduction and Discrimination

Kristina Froehlich[a,#], Saima Nasir[a,b,#], Mubarak Ali[a,b,*], Patricio Ramirez[c], Javier Cervera[d], Salvador Mafe[d], and Wolfgang Ensinger[a]

[a]*Dept. of Material- and Geo-Sciences, Materials Analysis, and Center of Synthetic Biology, Technische Universität Darmstadt, Alarich-Weiss-Str. 02, D-64287 Darmstadt, Germany*

[b]*Materials Research Department, GSI Helmholtzzentrum für Schwerionenforschung, Planckstrasse 1, D-64291, Darmstadt, Germany*

[c]*Dept. de Física Aplicada. Univ. Politècnica de València. E-46022 Valencia, Spain*

[d]*Dept. de Física de la Terra i Termodinàmica, Universitat de València, E-46100 Burjassot, Spain*

# Equal contributions

*Corresponding authors:

Email address: m.ali@gsi.de

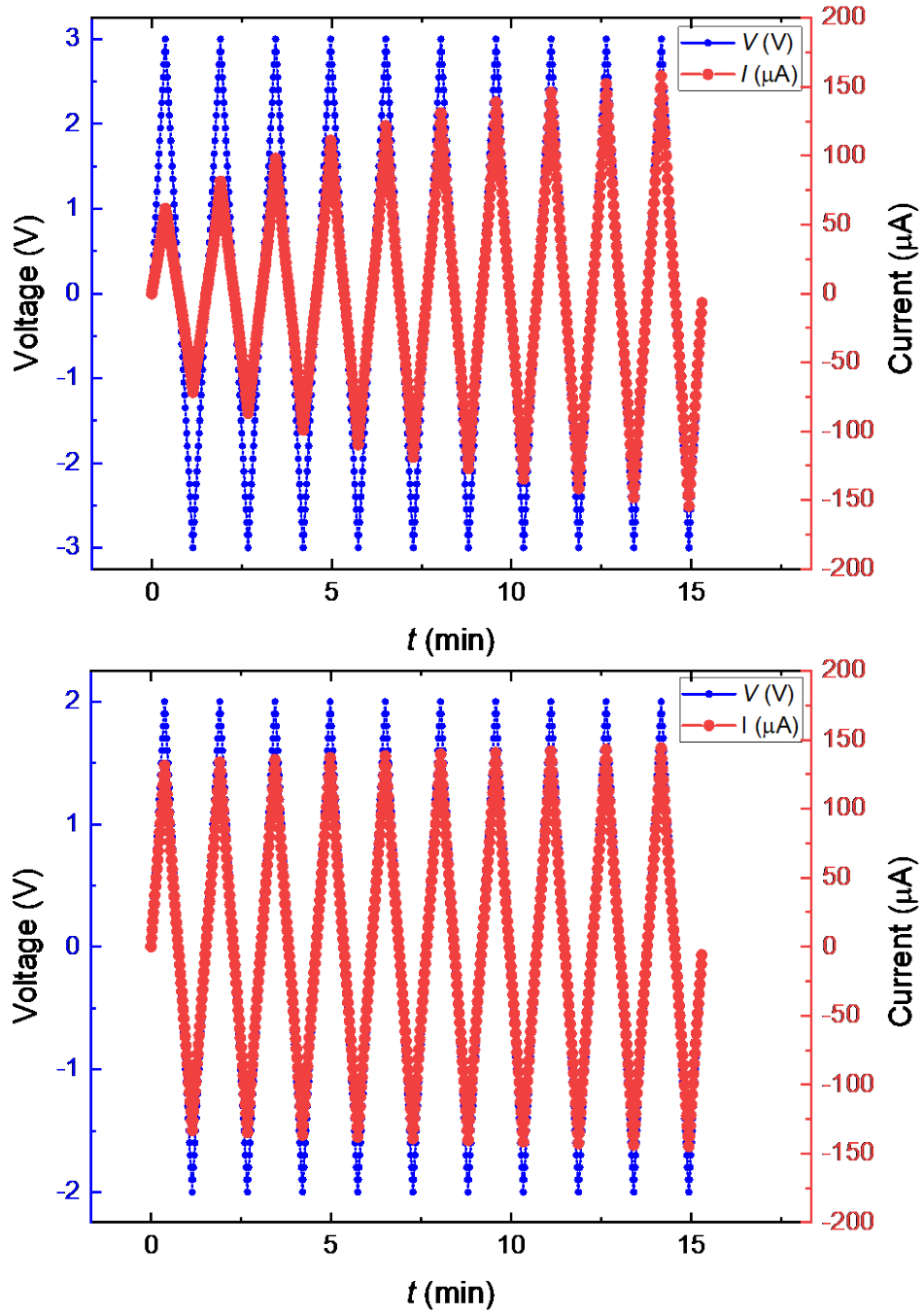

Fig. S1. Changes in the ion current versus time for triangular voltages of amplitudes 3 V (A) and 2 V (B) in the case of a DMF-treated PI membrane irradiated with heavy ions of fluence 10^9 ions/cm^2.

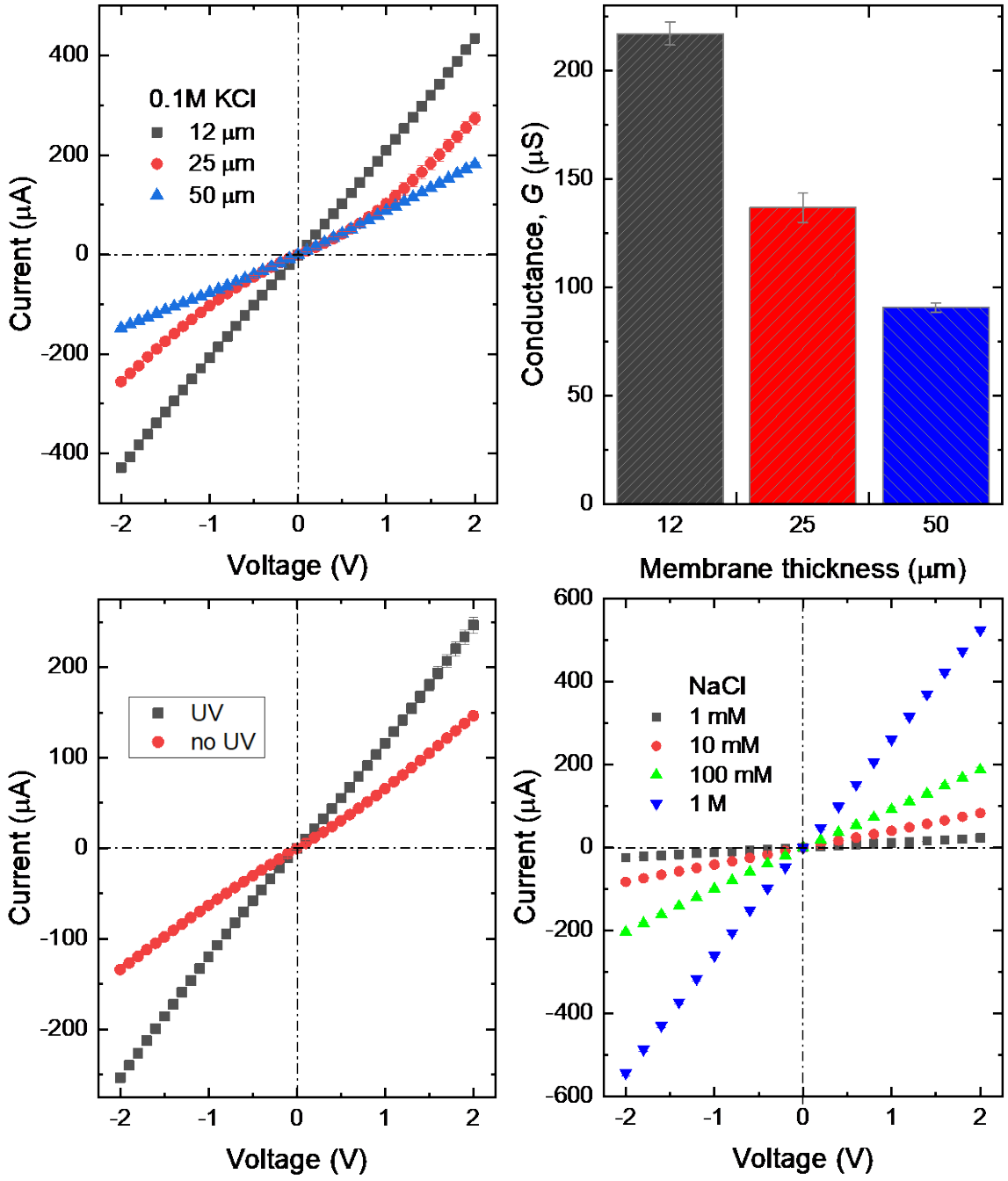

Fig. S2 *I–V* curves for DMF-treated membranes of different thickness in a 100 mM KCl solution (A). The ion conductance at 2 V obtained from the corresponding *I–V* curves for different PI membrane thickness (B). *I–V* curves for a 100 mM KCl solution and UV treated and non-UV treated PI membranes irradiated with a fluence 10^9 ions/cm^2 and treated with DMF (C). *I–V* curves of DMF-treated PI membranes at different NaCl concentrations (D).

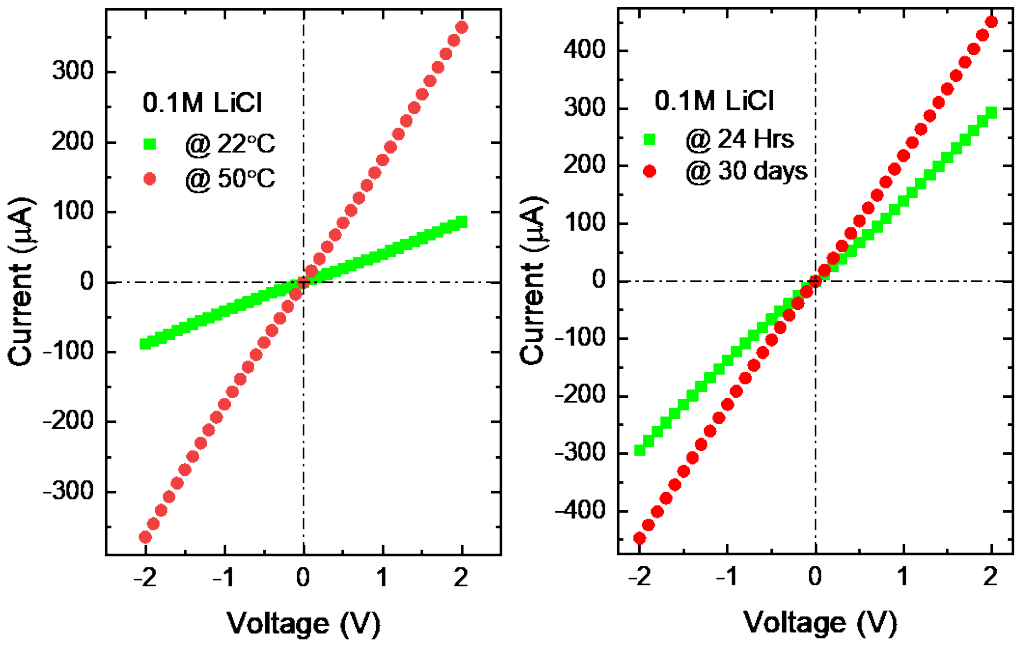

Fig. S3. *I–V* curves of MeOH- (A) and DMF (B) –treated PI membranes (10^9 pores /cm^2) prepared at room temperature (22°C) and high temperature (50°C) in 100 mM LiCl solutions under symmetrical electrolyte conditions.

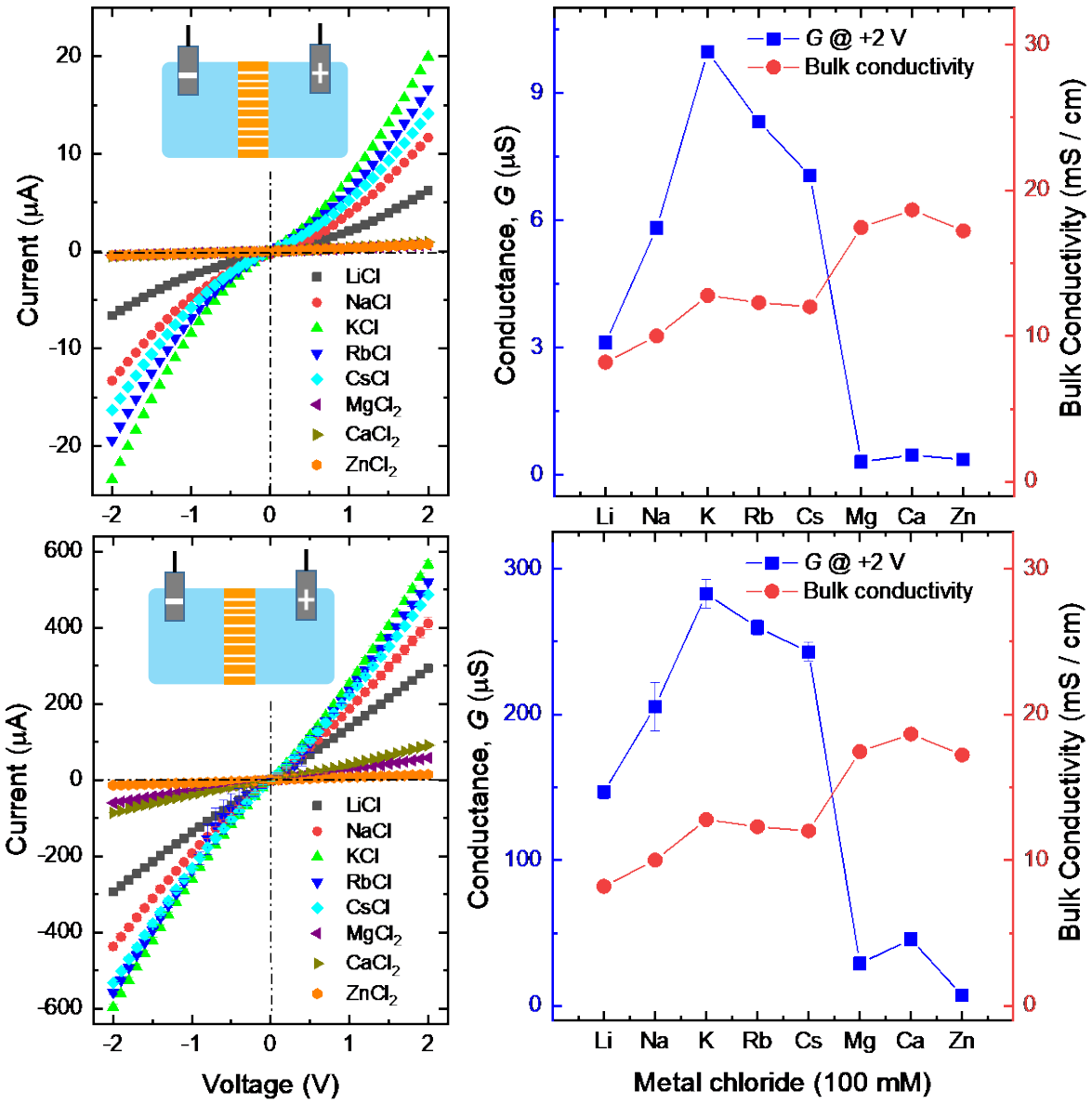

Fig. S4. *I–V* curves (left) and ion conductances (right) of MeOH (A and B) and DMF (C and D) –treated PI membranes in 100 mM metal chloride solutions under symmetrical electrolyte conditions. The bulk conductivities are shown for the sake of comparison. In most of the measurements the error bars are smaller than the size of the symbol.

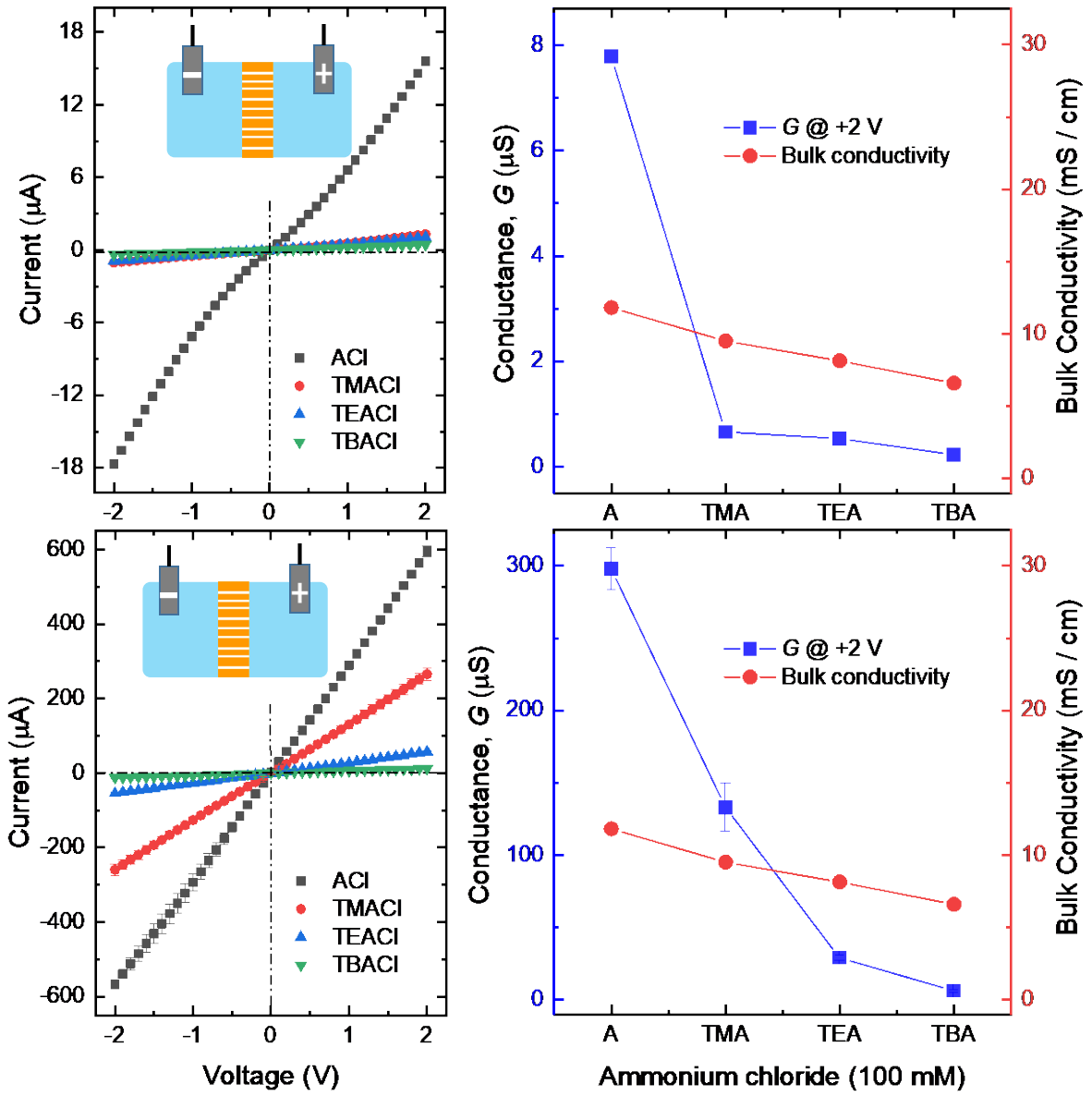

Fig. S5. *I–V* curves (left) and ion conductances (right) of MeOH (A and B) and DMF (C and D) –treated PI membranes in 100 mM alkylammonium chloride solutions under symmetrical electrolyte conditions. The bulk conductivities are shown for the sake of comparison.

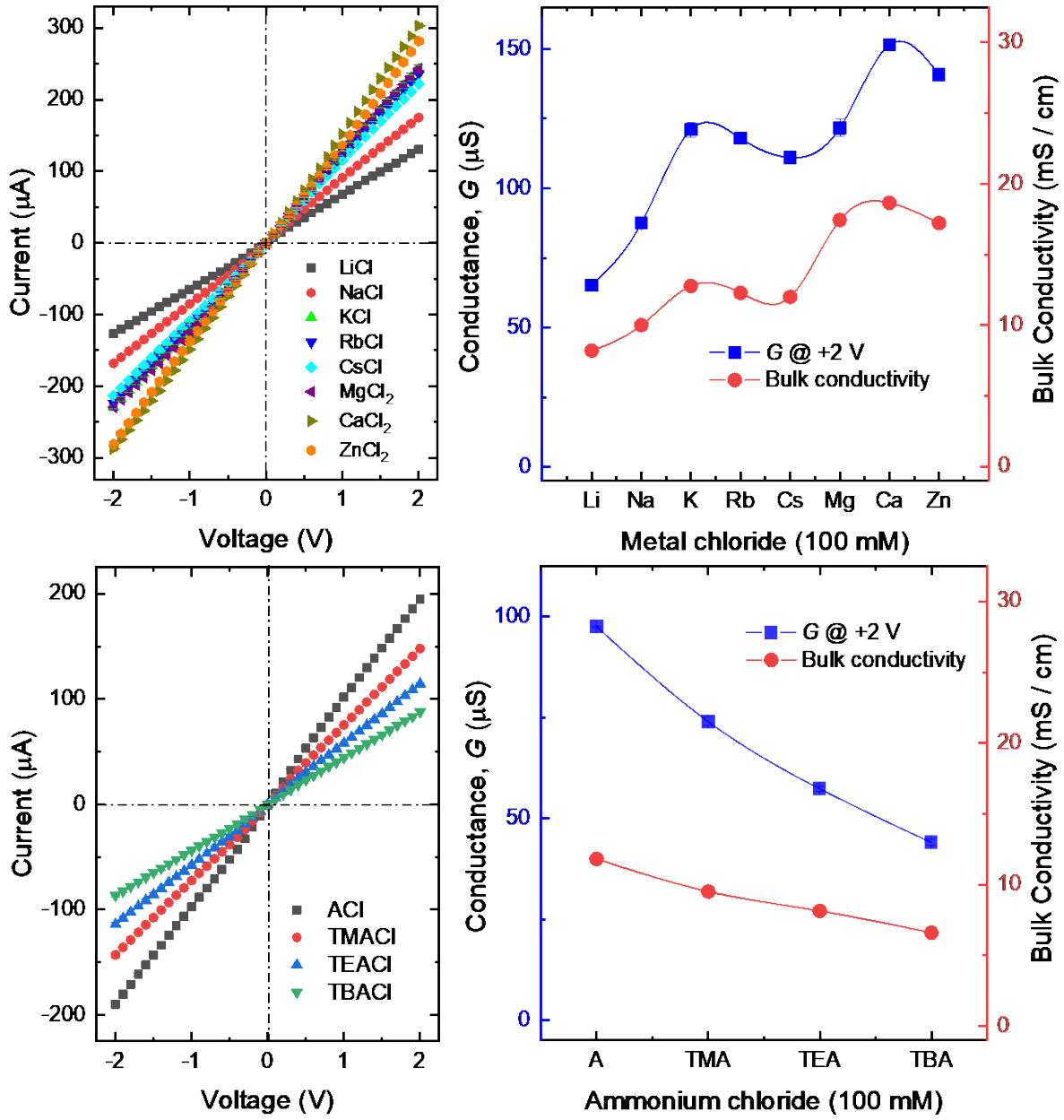

Fig. S6. *I–V* curves (left) and ion conductances (right) of a PI membrane chemically etched with NaOCl in 100 mM metal chloride solutions (A and B) and alkylammonium chloride (C and D) under symmetrical electrolyte conditions. The bulk conductivities are shown for the sake of comparison. In most of the measurements the error bars are smaller than the size of the symbol.

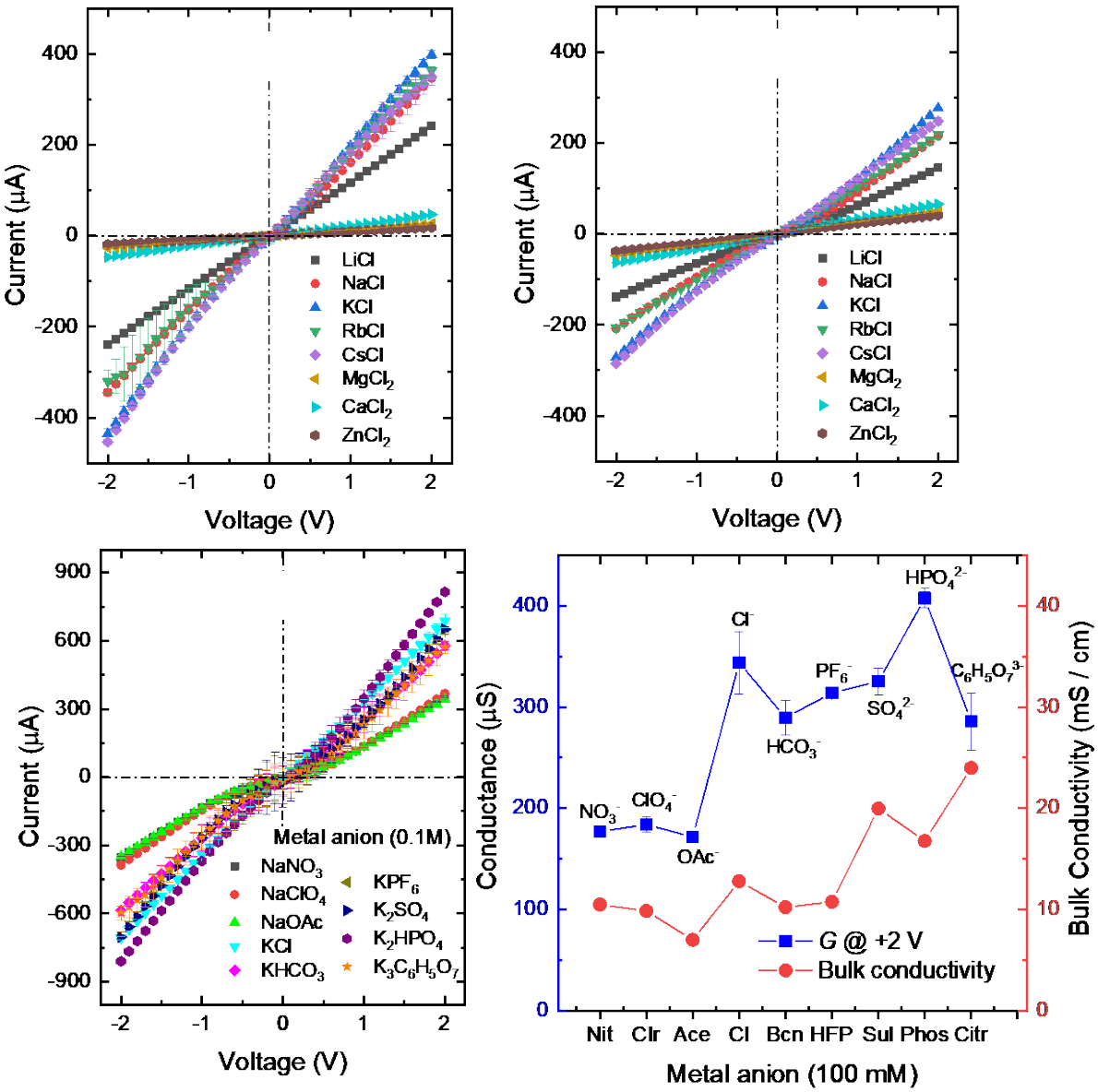

Fig. S7 *I–V* curves of DMF-treated PI membranes of fluence 10^9 ions/cm^2 in 100 mM alkali chloride solutions at close to neutral and acidic conditions (A and B). *I–V* curves and ion conductances of the membranes in aqueous electrolyte solutions of different anions under symmetric electrolyte conditions. (C and D)**.** The bulk conductivities are shown for the sake of comparison.

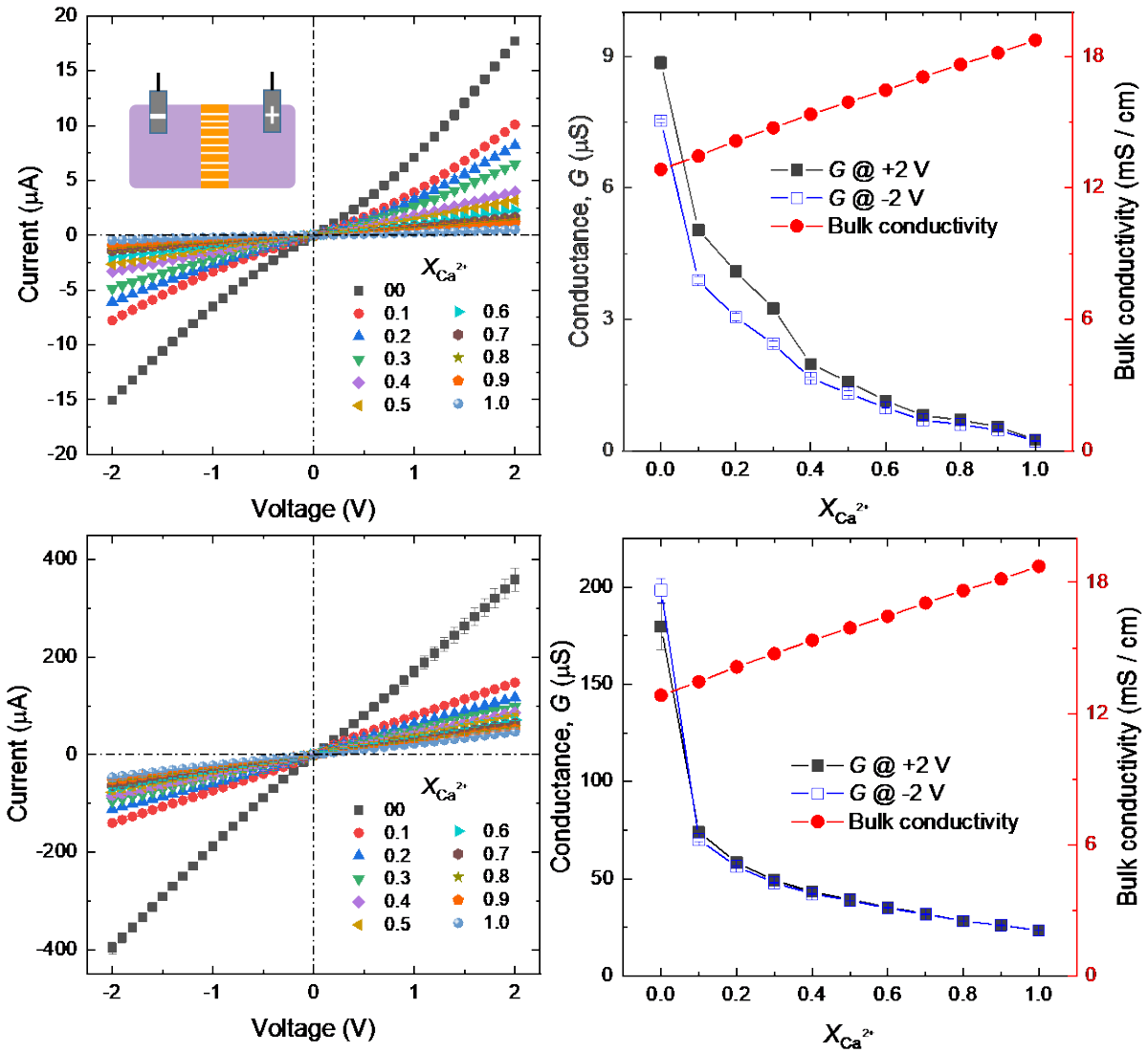

Fig. S8. *I–V* curves and ion conductances of MeOH (A and B) and DMF (C and D) –treated PI membranes at different Ca^{2+} mole fractions with [KCl + $CaCl_2$] = 100 mM and symmetric electrolyte conditions. The bulk conductivities are shown for the sake of comparison.

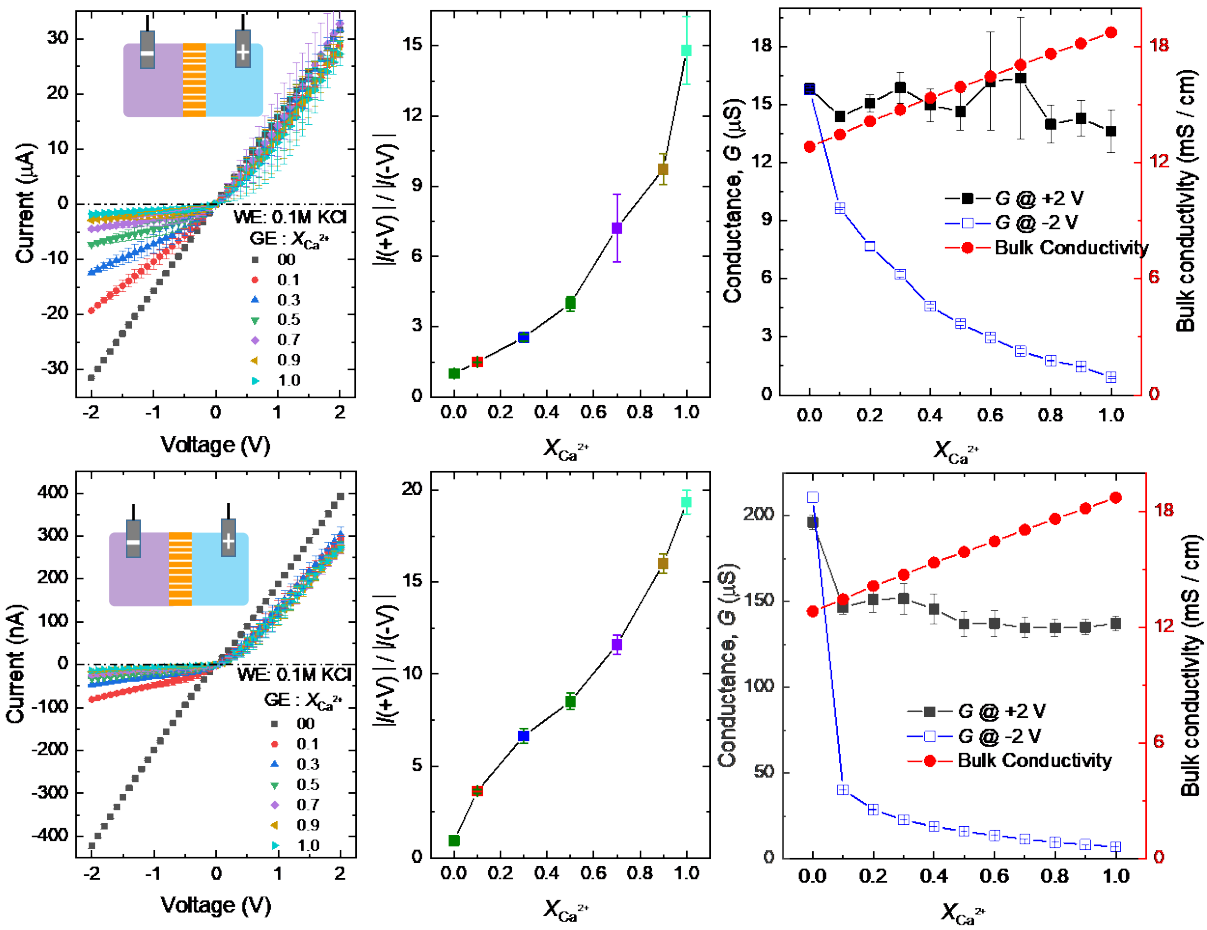

Fig. S9. *I–V* curves, rectification ratios, and ion conductances of MeOH (A–C) and DMF (C–F) –treated PI membranes at different Ca^{2+} mole fractions with [KCl + $CaCl_2$] = 100 mM and asymmetric electrolyte conditions. WE makes reference to the working electrode bathed in a 100 mM solution while GE corresponds to the ground electrode bathed in different solutions. The bulk conductivities are shown for the sake of comparison.